Medical Engineering & Physics 34 (2012) 972–981

Contents lists available at SciVerse ScienceDirect

Medical Engineering & Physics

journal homepage: www.elsevier.com/locate/medengphy

Wireless instrumentation system based on dry electrodes for acquiring EEG signals

Nuno Sérgio Dias[a,b], João Paulo Carmo[c,*], Paulo Mateus Mendes[c], José Higino Correia[c]

[a] Life and Health Sciences Research Institute (ICVS), School of Health Sciences, University of Minho, Braga, Portugal
[b] ICVS/3B's - PT Government Associate Laboratory, Braga/Guimarães, Portugal
[c] University of Minho, Dept Industrial Electronics, Campus Azurem, 4800-058, Portugal

ARTICLE INFO

Article history:
Received 14 February 2011
Received in revised form
22 September 2011
Accepted 1 November 2011

Keywords:
Wireless acquisition system
Wireless EEG
Dry electrodes
Neural signals

ABSTRACT

This paper presents a complete non-invasive Wireless acquisition system based on dry electrodes for electroencephalograms (WiDE-EEG) with emphasis in the electronic system design. The WiDE-EEG is composed by a 2.4 GHz radio-frequency (RF) transceiver, biopotential acquisition electronics and dry electrodes. The WiDE-EEG can acquire electroencephalogram (EEG) signals from 5 unipolar channels, with a resolution of 16 bits and minimum analog amplitude of 9.98 μV_{pp}, at a sampling rate of 1000 samples/s/channel and sends them to a processing unit through RF in a 10 m range. The analog channels were optimized for EEG signals (with amplitudes in the range 70–100 μV) and present the following characteristics: a signal gain of 66 dB and a common mode rejection ratio of 56.5 dB. Each electrode is composed by 16 microtip structures that were fabricated through bulk micromachining of a (1 0 0)-type silicon substrate in a potassium hydroxide (KOH) solution. The microtips present solid angles of 54.7°, a height of 100–200 μm and 2 μm spaced apart. The electrodes have a thin layer (obtained by sputtering) of iridium oxide (IrO) to guaranty their biocompatibility and improve the contact with the skin. These dry electrodes are in direct contact with the electrolyte fluids of the inner skin layers, and avoid the use of conductive gels. The complete WiDE-EEG occupies a volume of 9 cm × 8.5 cm × 1 cm, which makes it suitable for true mobility of the subjects and at the same time allows high data transfer rates. Since the WiDE-EEG is battery-powered, it overcomes the need of galvanic isolation for ensuring patient safety observed on conventional EEG instrumentation systems. The WiDE-EEG presents a total power consumption of 107 mW, divided as follows: the acquisition system contributes with 10 mW per channel, whereas the commercial MICAz module contributes with 57 mW (e.g., 24 mW from the microcontroller and 33 mW from the RF chip). The WiDE-EEG also presents autonomy of about 25 h with two class AA 1.5 V batteries.

1. Introduction

Today, wireless modules (composed by sensors, control and processing electronics, a RF transceiver and an associated antenna) find a great field of applications. Such applications are those found in wireless sensors networks (WSNs) [1–6], whose methodology is to acquire data from sensors through wireless modules, temporarily store the data, and send it by radio-frequency (RF) to an external station (e.g., a PDA, other mobile devices, or even a fixed station) for further processing. RF modules have been used with success in the monitoring of human-body information, where the biomedical data of individuals is wirelessly transmitted to a central processing unit (e.g., a base-station) [7–10]. In a conventional system (see Fig. 1), the electroencephalogram (EEG) electrodes are placed in standard locations of a classic braincap, and connected to an external (and bulky) central processing unit. Due to the high number of electrodes, many wires restrain the patient that stays next to the central processing unit during the exam. In this context and in contrary to the classic approaches, new solutions based on wireless EEG modules fits the clinical requirements for an easy placement and removal of the electrodes in a braincap, especially with dry electrodes. Thus, wireless EEG is an important breakthrough in the monitoring, diagnosis and treatment of patients with neurological diseases because it allows patients to maintain their mobility during the exam.

This paper presents a complete non-invasive (without skin abrasion and electrolytic gel) wireless acquisition system (WiDE-EEG) to acquire EEG signals, which contains the necessary electronics and electrodes. The WiDE-EEG uses dry sputtered iridium oxide (IrO) electrodes that can penetrate the outer skin layer (which is 5–10 μm thick and it is called *stratum corneum*) for avoiding its high-impedance characteristics and the use of conductive gel.

* Corresponding author. Tel.: +351 253 510190; fax: +351 253 510189.
E-mail address: jcarmo@dei.uminho.pt (J.P. Carmo).

1350-4533/$ – see front matter © 2011 IPEM. Published by Elsevier Ltd. All rights reserved.
doi:10.1016/j.medengphy.2011.11.002

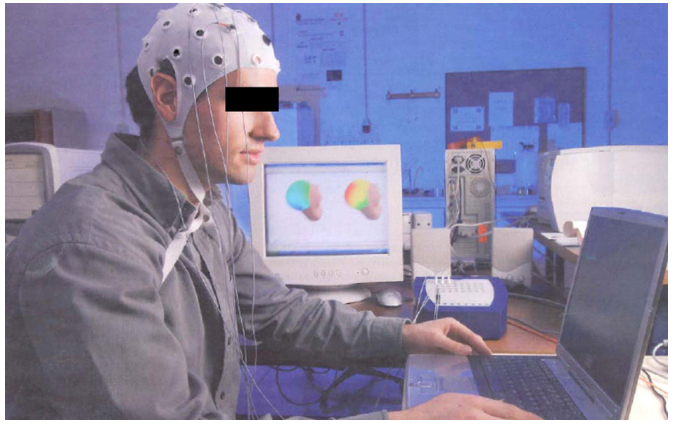

Fig. 1. Photograph showing an individual using a wired classic EEG braincap with silver/silver chloride (Ag/AgCl) electrodes [11].

2. System overview

Recent advances in the biomedical field related with medicine and biology have been demanding more sophisticated electrode fabrication technologies [12]. Electrical activity occurs between neurons as well as in the muscles (e.g., heart) and nerves. The biopotential electrodes, jointly with acquisition systems, sense that electrical activity and make it accessible either for clinical or research trials. Sintered silver/silver chloride (Ag/AgCl) ring electrodes for guaranteeing low-constant transition resistance are the most commonly found in EEG sessions with patients [13], but a electrolytic gel is needed in order to reduce the impedance of each electrode (e.g., to bypass the *stratum corneum* isolation properties as illustrated in Fig. 2a) and minimizing unwanted noise in the recording [14]. Moreover, the gel also has an important role for providing the necessary ions to support the redox reaction at the electrode-skin interface that is responsible for the very stable half-cell potential and subsequent low noise performance. Often some abrasion of the skin is required to remove dead skin cells (which have small water contents [15]) and to reduce the impedance. After skin preparation, electrodes are placed on the skin and usually some viscous saline gel, electrolyte, is added to improve the contact between the electrode and skin [16]. As an example, the preparation time for 32 standard EEG electrodes (as it is the case of Ag/AgCl electrodes) may take up to 45 min. Therefore, biopotential electrodes with microtips that are able to penetrate the outer skin layer and directly interface to the electrolytic fluids (abundance of some chlorides like NaCl) of living epidermis are of great interest (Fig. 2b). This reduces the preparation time and discomfort of patients. A microtip is presented in Fig. 3a and a standard sintered Ag/AgCl ring electrode is presented in Fig. 3b.

The WiDE-EEG presented in this paper uses dry electrodes to be paced on the individual's scalp without the need of electrolyte gel or skin abrasion. Each electrode is an array with 4 × 4 microtips covered with a thin layer of iridium oxide (IrO). The coated layer of IrO was obtained by DC-sputtering after bulk micromachining through a wet etching process with undercut in a potassium hydroxide (KOH) solution. As depicted in Fig. 3a, each microtip in the array is at least 100 μm high in order to pass through the *stratum corneum*. It is important to mention that since the length of microtips are smaller than 200 μm (for providing the penetration of the outer skin layer, e.g., the *stratum corneum* with a thickness of 10 μm), the electrodes never reach the *dermis* region (where the sensing nerves are located). In spite of skin penetration, this feature justifies the non-invasive character of the micro-tips electrode because

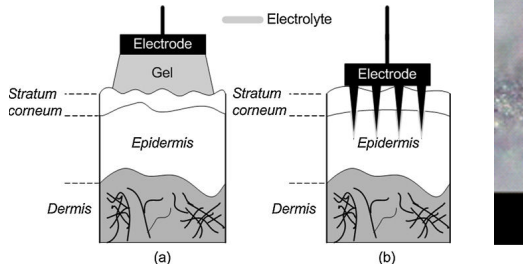

Fig. 2. Application of biopotential electrodes: (a) standard EEG electrode and (b) EEG electrode with microtips.

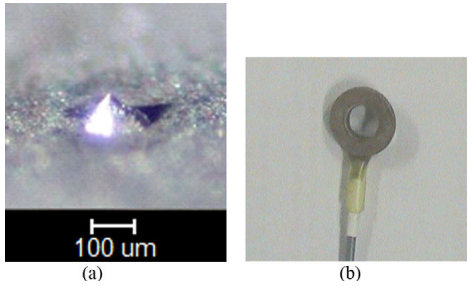

Fig. 3. (a) Magnified photograph of a microtip with pyramidal shape, and (b) a standard sintered Ag/AgCl ring electrode.

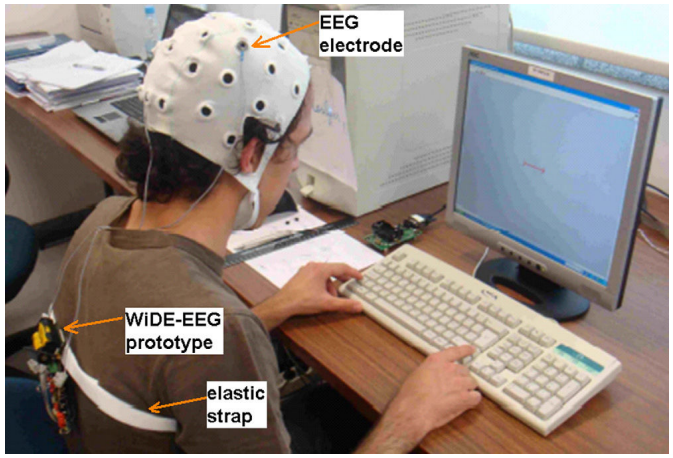

Fig. 4. A subject with a WiDE-EEG prototype fixed with the help of an elastic band (the white strap) on the thorax region. An ordinary EEG braincap was used for fixing the EEG electrodes in the head during the tests.

the patient never feels pain. Fig. 4 shows how a WiDE-EEG prototype and the electrodes are placed on the head of a subject for doing the tests. An elastic band with a form of strap is placed in the thorax region for fixing the WiDE-EEG module then, an ordinary braincap helps the electrodes positioning and fixation. The risk of infections is another important topic when designing electrodes, because the *stratum corneum* is a natural barrier in the skin. In this context, these electrodes do not increase the risk of infection the incision resultant from skin penetration is small enough (less than 150 μm) to allow the close up after removal (due to the rapid coagulation).

Several companies have been offering radios (motes) and sensor interfaces for development applications [17,18]. The motes are battery-powered devices that run specific software (e.g., TinyOS [17,18]). In addition to running the networking stack software, each mote can be easily customized and programmed, since it runs an open-source operating system which provides low-level event and task management as well as sensor data conditioning. The mote processor/radio families are ready for working in the 2.4 GHz ISM band and supporting IEEE 802.15.4 and ZigBee protocols. The WiDE-EEG development involved a combination of hardware and software design, utilizing both custom solutions and commercial off-the-shelf (COTS) components [18]. As illustrated in Fig. 4, the emitter mote runs software components that were developed to control the acquisition electronics, to handle all the communication with the acquisition electronics, to assemble the data packet, to implement the medium-access control (MAC) protocol and to send the data packets wirelessly to the receiver mote. The MAC protocol was optimized and implemented in the MICAz [19] platform to allow high-data throughput [20]. The receiver mote provides a serial connection to the central processing unit (e.g., a personal computer – PC) serial port. The central processing unit receives the acquired data through software server-client architecture applications. In this context and as further presented, the architecture of the WiDE-EEG differs from others previously presented [21,22] because it combines several COTS parts (CPU and RF transceiver) with dry electrodes. As presented further, these wireless modules allows the expansion for acquiring and coding analog samples with 16 bits in the following situations: (1) using the same ADC is possible to expand the system up to eight EEG channels sampled at the speed of 2k sps or (2) up to 16 EEG channels, keeping the sampled speed in the original value of 1000 sps.

3. Hardware and software

3.1. The wireless link

The wireless connection between the WiDE-EEG device and the central processing unit (see Fig. 5a) is based on two radio modules MICAz from a third party supplier [19], which was previously mentioned as motes. These devices were selected due to their flexibility to implement wireless sensors networks in an expedite way.

A mote allows the establishment of wireless links between the WiDE-EEG and central processing unit for data transmission purposes, and to control both the analog and the digital electronics of WiDE-EEG. This module receives the data from the EEG acquisition board. This board is responsible for picking up the EEG signals from the electrodes, amplify, convert them to digital format and send the data to the mote. The other mote is used as a receiver, and it is in the central processing unit. A serial interface allows the receiver mote to communicate with the central processing unit. Fig. 5b shows a block diagram of a mote (the analog and digital input/output features of the processor were used to control the electronics responsible for the acquisition of the EEG signals), the data is processed by a microcontroller Atmega128 (from Atmel) with 512 kb of flash memory. This microcontroller has analog and digital inputs/outputs that enable this module to communicate with an extra instrumentation board. An I^2C interface is also provided by the microcontroller for communication with external hardware. The motes also contain a system-on-chip (SoC) platform (with a Chipcon's radio chip model CC2420 compliant with IEEE 802.15.4), which allows wireless communications at 2.4 GHz [17].

The mote in Fig. 5c presents the dimensions 5.8 cm × 3.2 cm × 1.5 cm including two 1.5-V batteries. The receiver mote communicates with the central processing unit by way of a RS232 serial communication. In Fig. 5c, a regular PC was used as central processing unit.

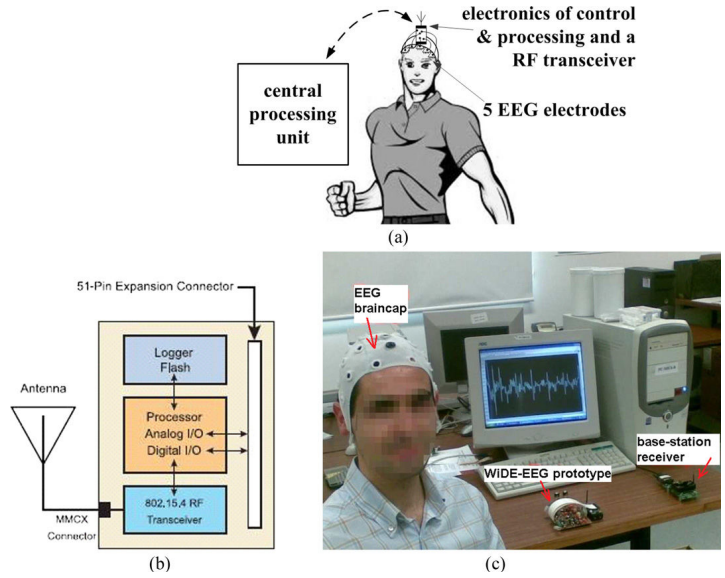

Fig. 5. (a) System overview of the WiDE-EEG, where it can be seen a set of 5 IrO electrodes, the control electronics (digital electronics) and processing (analog electronics), a RF transceiver at 2.4 GHz with an associated antenna. The communication between the WiDE-EEG and the central processing unit is done wirelessly. (b) A mote's block diagram, where the block of the processor (with analog and digital inputs) controls the electronics used to acquire the EEG signals. (c) A photography of a complete WiDE-EEG with an attached mote, which communicates with the receiver mote (i.e., connected to the central processing unit through a RS232 serial communication).

The receiver mote operates on a standard TinyOS software component that receives packets and broadcasts them via a serial port or radio. The data-acquisition software component implements a five channel signal-acquisition and an algorithm that assemble each data block that will be sent. Each data block contains a header and data fields. The header has the source mote ID, the last sample number, and the cyclic redundancy check (CRC). The data field is fulfilled with 20 samples of 20 bits for every channel.

3.2. The acquisition system

The acquisition system is based on a single-ended structure where each of the amplified signals is sensed by one of the 5 signal electrodes and a reference electrode. Previous brain–computer interface experiments involving the optimization of EEG sensor sets for task discrimination resulted in classification errors as low as 12.5% with only 5 EEG electrodes and thus, reducing the feature set dimensionality. However, the 8 bits ADC allows future upgrading of the number of EEG channels. Fig. 6a shows the block diagram of the acquisition system, where it can be seen that the potential of each electrode is 1.25 V level-shifted through a summing non-inverter amplifier. This level-shift is necessary for allowing the use of a single-rail power supply without compromise the acquisition of differential signals. This amplifier scheme is based on an AD822 (whose schematic is illustrated in Fig. 6b) which accepts single-supply and offers rail-to-rail FET-input operational amplifiers. This operational amplifier was selected because it presents low-power (each operational amplifier absorbs 800 μA) thus, it is suitable for battery-powered medical instrumentation. Also, its input impedance is about 100 TΩ which provides a high-impedance input stage (due to their implementation using FET transistors), which allows low polarizing input currents (bellow 25 pA).

Each of the 5 channels (at the instrumentation amplifiers, AD627) is measured as a potential difference between itself and the reference channel (the SGND electrode). So, the operational amplifier output of the SGND electrode connects to all the inverting inputs of the instrumentation amplifiers (IAs). The AD627 integrated circuit can work in single and dual-supply although 3.3 V is the only power supply potential available in this system from two AA batteries. Thus, rail-to-rail voltages can be provided by the AD627, making this IA suitable for application in EEG medical instrumentation. The gain of the IA was selected to be 10. The reference potential of each channel signal at the IA output is 1.25 V, instead of the potential of the reference electrode, because the electrode potentials were level-shifted at the high-impedance input stage. Ideally, this level shifting voltage should be half of the dynamic range available for the ADC, in order to adjust the reference voltage, V_{ref} [V] to half of the value provided by the batteries power-supply (i.e., 1.5 V). This voltage level constitutes the DC value of the amplified signal, thus any variation will result on errors in the sampled signal. It is desirable to avoid voltage dividers for getting voltage references because their unregulated nature can result on undesirable variations. This happens due to a multiplicity of factors, such as drops on the supply voltage (due to the battery discharge), unexpected variations on load impedances (due to the number of electronic components for supplying) and temperature drifts. These were few reasons behind the selection of a voltage regulator from

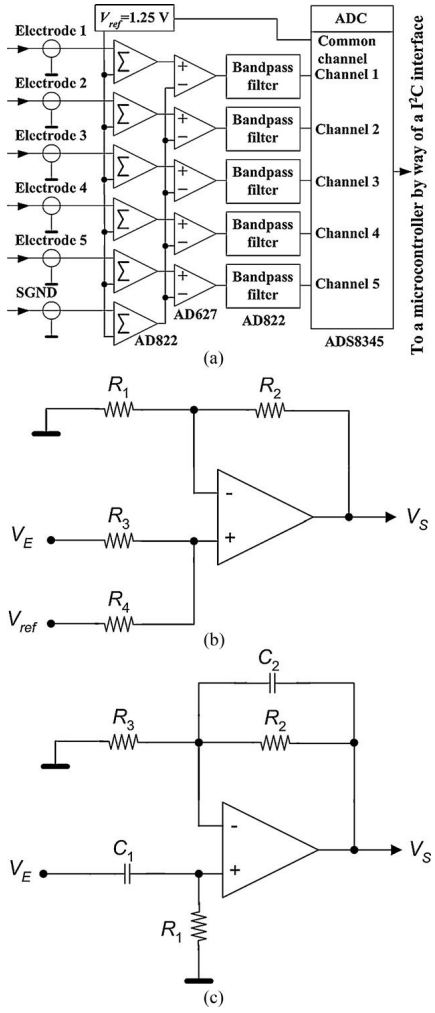

Fig. 6. (a) The block diagram of the acquisition system. Schematics of the electronic circuits of (b) non-inverting adders (R_1 = 100 kΩ, R_2 = 100 kΩ, R_3 = 4.7 MΩ and R_4 = 4.7 MΩ), and of (c) an individual bandpass filter. Both electronic circuits used the operational amplifier AD822 for their implementation (R_1 = 470 kΩ, R_2 = 200 kΩ, R_3 = 300 kΩ, C_1 = 0.5 μF and C_2 = 22 nF).

Texas Instruments supplier for providing the reference voltage for the instrumentations. The electronic component with the reference REF3212 with output voltage of 1.25 V was the selected voltage regulator because it was the one with the nearest output voltage next to the desirable value of 1.5 V. This voltage regulator provides a very stable output voltage with a maximum variation of only 7 parts per million per °C, measured in the temperature range of [0, 125] °C, as well as an high accuracy (with a maximum error of 0.01%), a low quiescent current of 100 μA (do not compromising with an excessive amount the useful life of batteries) and a low dropout voltage of 5 mV (i.e., less or equal than 0.4%, when compared with the reference voltage).

The next stage is composed by 5 bandpass filters that eliminate the interference from the surrounding environment as well as the interferences induced by the other components. The filters are composed by a bandpass filter with 100 Hz of bandwidth and an amplifier with a gain of 100. These filters were implemented again with the AD822 operational amplifier. The resulting signal after two amplifications is in the range of ADC (implemented with an ADS8345), e.g., 0–3.3 V. The resolution conversion (maximum) of this low-power ADC is of 16 bits. Fig. 6c shows the schematic of the electronic circuit used for implementing each band-pass filter. The upper and lower cutoff frequencies of the filter (f_1 and f_2 respectively) can be fully customized by selecting the passive components:

$$f_1 = \frac{1}{2\pi R_1 C_1} \quad (1)$$

$$f_2 = \frac{1}{2\pi R_2 C_2} \quad (2)$$

This kind of filter has the advantage to present gain, which can also be customized by selecting the appropriated passive components:

$$G = 1 + \frac{R_2}{R_3} \quad (3)$$

It must be noted the fact of the gain to be uncoupled from the upper and lower cutoff frequencies, because R_3 gives the freedom degree necessary to select the gain without affecting any cutoff frequency.

The resulting signal from each of the 5 channels is converted to digital format using the ADC at a data sampling rate of 1000 samples/s (maximum values). It digitalizes 5 single-ended signals between the outputs of the IA and a common-reference which is the 1.25 V. The ADC data registers are available for reading through an I²C interface. As it was referred in the previous section, the task to manage the configuration registers of the ADC belongs to the mote. The mote also assembles the data packets and sends them wirelessly to another similar mote (e.g., the receiving mote in the central processing unit).

3.3. Experimental results

The global gain of each analog channel was designed to be distributed by the different blocks in the chain. The gain of the voltage level shifting circuits is always unitary. The maximal allowable gain of 66 dB is obtained with 14 dB in the IA and 52 dB in the passband circuit. The main advantage was to keep a reduced gain in the IA, because the highest CMRR values are achieved for the smallest gains. This common voltage is due to the impedance difference between the skin and the electrode, and it is the main cause of interference in the IA. A sinusoidal wave with 2 V_{pp} with 15 Hz was connected in two analog channels (after adjusting the gain to 34.8 dB, i.e., 14 dB for the IA and 20.8 for the passband filter after replacing R_3 = 200 kΩ by another with 20 kΩ), and both the input and the output voltages were measured. The ratio between the voltages measured in the outputs (150 mVpp) to the input voltage was 0.075 (−22.5 dB). Because the differential gain was adjusted to be 34.8 dB, the ratio between the differential and the common gains resulted in 666.66 (56.6 dB). The explanation for this discrepancy is the difficulty to generate frequencies below 3 Hz with low amplitudes with the available signal generator for validating the filter behavior. As it was expected, the maximum measured gain in the passband was measured to be about 35 dB.

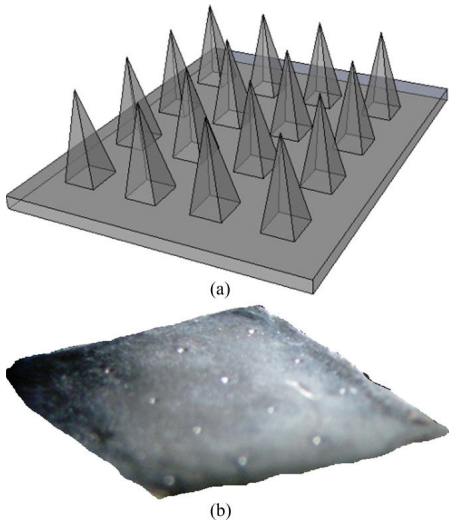

Fig. 7. (a) The schematic of IrO electrode with 4 × 4 array microtips, and (b) an IrO electrode with 4 × 4 microtips and detail of the structure of a microtip [29].

In theory, the minimum amplitude is imposed by the ADC resolution, whose value for the maximum gain (for a gain of 2005 or 66 dB) is about 19 nV (which corresponds to an output of $(2^{16} - 1) \times 2005 \times 19\,nV = 2.4966\,V$). However, this value is optimistic and unrealistic because do not take in account the effect of noise. A set of tests were done on all EEG channels, which consisted on connecting all inputs to the reference electrode (SGND in Fig. 6a) except one and measuring the maximum voltage peak produced by the noise. The respective voltage peak in the input (referred to the node before the non-inverting amplifier responsible for doing the voltage-level shift of 1.25 V) was also measured. The tests done for the maximum gain of 66 dB showed maximum peak voltages of 550 μV_{pp} and 9.98 μV_{pp} in the output and input, respectively. The actual minimum amplitude (i.e., the system resolution) is limited by the noise voltage (i.e., cannot be smaller than the maximum voltage peak produced by the noise) and results on 9.98 μV_{pp}, which corresponds to a value 45.3 dB (more than two orders of magnitude) above the theoretical 19 nV.

4. The EEG electrodes

The needle-shape electrodes in Fig. 2b provide microtip length of about 100–200 μm for providing the penetration of the outer skin layer (i.e., the *stratum corneum*) that is 10 μm thick.

Each microtip in the dry electrode has a three dimensional structure, which is fabricated by wet-etching process in silicon through a liquid solution of potassium hydroxide (KOH). The microtips desired shape is obtained by the undercut effect in the etching, where the planes of fast etching are revealed. In this context, Fig. 7a shows a schematic of an IrO electrode composed by an array of 4 × 4 microtips.

The etching process employed is anisotropic, with an angle of 54.7° between the [1 1 1] and the [1 0 0] planes [23–28]. The etching solution of KOH was by 30% at a temperature of 87 °C, ensuring an etching rate of 1.6 μm/min. The microtip pyramidal structure

Table 1
Performance comparison of neural wireless acquisition systems.

Type of construction	Institution								
	WIDE-EEG COTS	Cleveland Medicine COTS	UCSD Personalized	Michigan Personalized	Duke COTS	Zhejiang University COTS	Tokyo University Personalized	UCLA COTS
Number of EEG channels	5	8	1 (daisy chain expandable)	4	12	2	1	6
Signal resolution	16 bits	12 bits	–	–	12 bits	12 bits	–	8 bits
CMRR	77 dB	–	–	77 dB	–	126 dB	90 dB	–
System resolution	9.98 μV_{pp}	–	3.8 μV	0.1–5 mV	–	–	–	0.06–15 mV
Maximum detectable frequency	500 Hz	125 kHz	100 Hz	10 kHz	15 kHz	4.5 kHz	–	240 Hz
Maximum signal gain	66 dB	–	46 dB	39 dB	30 dB	40 dB	–	46 dB
Telemetry link frequency	2.4 GHz	902–928 MHz	2.4 GHz	94–98 MHz	2.4 GHz	2.4 GHz	80–90 MHz	916 MHz
Maximum baud-rate	250 kbps	40 kbps	–	–	–	70 kbps	–	9.6 kbps
Communication scheme	802.15.4	FSK	Bluetooth	Analog FM	802.11b	Bluetooth	Analog FM	FSK
Power supply	3 V (AA)	9 V	3 V	±1.5 V	3.3 V and 5 V	3.7 V	3 V	3 V
Power consumption per EEG channel	107 mW	–	300 mW	2.2 mW	333 mW	–	10 mW	66 mW
Range	10 m	45 m	–	0.5	9 m	100 m	16 m	2 m
System clock frequency	7.37 MHz	–	–	70–138 kHz	66 MHz	–	–	4 MHz
Dimensions [cm³]	9 × 8.5 × 1.0	6.4 × 5.1 × 1.0	0.17 diameter	1.7 × 1.2 × 0.2	5.1 × 8.1 × 12.4	3.6 × 2.2 × 0.4	5.1 × 0.8 cm²	2.6 × 2.6 × 1.8
Type of acquisition	Not invasive				Invasive			
Reference	This work	[33]	[34]	[35]	[36]	[37]	[38]	[39]

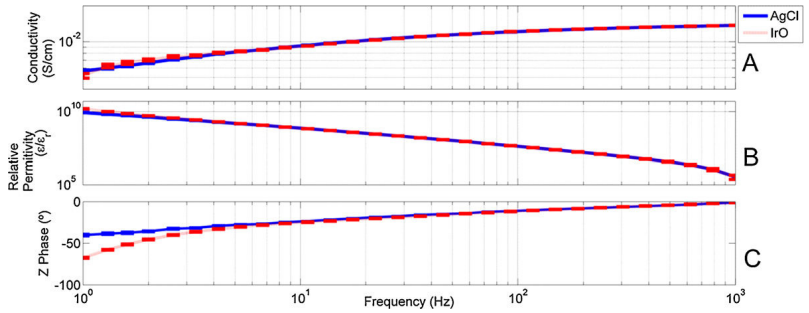

Fig. 8. For the whole frequency range (1–1000 Hz) [29]: (a) the conductivity, σ [S cm^{-1}] of the fabricated electrodes (solid line with blue colour) and of the control Ag/AgCl electrodes (dashed line with red colour); (b) the relative permittivity, ε_r, of the fabricated IrO electrodes (solid line with blue colour) and of the control Ag/AgCl electrodes (dashed line with red colour); and (c) the impedance phase measured for the fabricated IrO_2 electrodes (solid line with blue colour) and the control Ag/AgCl electrodes (dashed line with red colour). (For interpretation of the references to colour in this figure legend, the reader is referred to the web version of this article.)

due to the anisotropic process is presented in Fig. 7b. It can be observed the etching of square corners to a hexagonal shape as its final structure. The final microtip was 150–200 μm wider with a height around 100–200 μm.

The final fabrication step of the electrodes was its coverage with a conductive thin layer of IrO to pass through the *stratum corneum* (the non-conductive skin layer) and thus to minimize the resistivity of the interface electrode/skin. The IrO was also deposited to ensure the biocompatibility of the electrode.

Further details about the fabrication and characterization (for obtaining the electrochemical characteristics of the electrodes and their interface with the electrolyte) of the electrodes done by Dias et al. can be obtained in [29]. However, Fig. 8 shows the main results obtained from the experimental characterization. In electrochemical analyses, the admittance values, Y [S], are often assessed instead of the impedance values, Z [Ω], actually read, thus, $Y = Z^{-1}$, where $Y = G + jB$ and $Z = R + jX$ (G is conductance, B is susceptance, R is resistance, and X is reactance). The conductivity is the cell-geometry-independent value of the conductance, G, and usually assumed as the reverse of the resistivity (i.e., material property that is the cell-geometry-independent value of the resistance). The measurements showed that the conductivity ranges from around 5 mS cm^{-1} at 1 Hz to almost 14 mS cm^{-1} at 1000 Hz (Fig. 8a). At frequencies bellow 3 Hz, the conductivity of IrO electrodes is significantly different from that found in Ag/AgCl electrodes. Both electrode types exhibit comparable conductivity for frequencies above 3 Hz. The relative permittivity, ε_r, is the cell-geometry-independent value of the susceptance, B, in respect to vacuum permittivity (e.g., $\varepsilon_0 = 10^{-11}/(36\pi)$ F cm^{-1}) and gives some insight about the amount of capacitive behavior of each electrode type. The AgCl electrodes relative permittivity ranges from 3.5×10^5 at 1 kHz up to 10^{10} at 1 Hz (Fig. 8b). The measurements done on frequencies below 3 Hz showed that the relative permittivity of IrO electrodes is slightly higher than AgCl electrodes. The plot (c) in Fig. 8 represents the impedance phase measured for both electrodes. The AgCl electrodes presented an impedance phase of −40° for 1 Hz that decreases with frequency until it gets around 0° for 1 kHz. The IrO electrodes manifested significantly higher impedance phase values (−67° for 1 Hz) for frequencies below 3 Hz.

5. The complete WiDE-EEG

The WiDE-EEG is composed by the microtip EEG electrodes, the acquisition circuitry and a mote. Up to 5 EEG electrodes (and the additional SGND) can be connected to the acquisition system, containing the analog electronics necessary to the processing of the acquired EEG signals. Then, a mote composed by a RF transceiver at 2.4 GHz and a microcontroller attached to a socket located in the backside of the acquisition system. This socket provides the I^2C signals to control the acquisition process of the individual EEG channels. Fig. 9 shows the circuit board of the EEG acquisition system: (a) the top view of the EEG acquisition system (with analog and digital electronics), showing the electronic components; the bottom view of the EEG acquisition system (b) without and (c) with the mote attached. The RF part (e.g., a MICAz mote [30]) of the WiDE-EEG starts a wireless transmission at the frequency of 2.4 GHz using the O-QPSK (Offset Quadrature Phase-Shift Keying) modulation allowing up to 62.5k symbols per second (62.5k sps). As guaranteed by crossbow manufacturer for a point-to-point, these features allow wireless communication at the maximum bit-rate of 250 kbps. This means that the full usage of the ADS8345 analog-to-digital converter (i.e., using the eight analog inputs to produce binary words with 16 bits) allows the sampling of 2000 samples per second per EEG channel (2k sps/EEG channel or a total of 8×2k sps, which is below the 100k sps ADC limit). The mote provides the possibility to select one of the 16 RF central frequencies, $f_k = 2400 + 5k$ [MHz] with $k \in \{1,2,\ldots,16\}$ for transmission. This *modulation* [31] scheme (orthogonal coding with QPSK modulation) combined with a chip-rate of 2M chips (according Viterby, a chip is a CDMA symbol used in the context of wireless communications for improving the error resilience, resulting in smaller transmission errors and fading sensitivities when the number of chips per effective information bit is increased [VITERBi]) per second (8k chips per bit or 32k chips per O-QPSK symbol). These features makes this scheme extremely reliable in the presence of both slow and fast multi-path [32], whose probability is very slow due to the patient is not allowed to be on more than 10 m (i.e., the patients are to be moving but confined in a limited space apart from the base-station).

The mote controls the circuit board of the EEG acquisition system as follows: in the beginning of the operation, a specific interrupt of the MICAz mote (i.e., the INT0 interrupt) is activated. Simultaneously, an internal timer for controlling the sampling rate and the EEG channel number is initialized. Then, the mote waits an interrupt for acquiring an analog sample from the selected EEG channel and for doing an analog-to-digital conversion (ADC). After an acquisition and an ADC conversion, the EEG channel is updated. After all the five EEG channels being acquired, their samples are stored in the internal memory of the MICAz mote. If the buffer

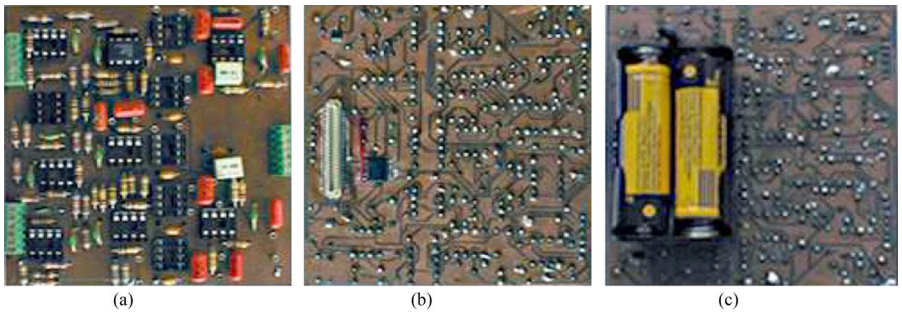

Fig. 9. The circuit board of the acquisition system, where it is possible to observe the electronic components: (a) the top view of the EEG acquisition system; and the bottom view of the EEG acquisition system (b) without and (c) with the mote attached (but only shows the two class AA batteries for supplying the whole system comprising the RF + control and the acquisition parts).

is not full and is able to accommodate an additional set of five EEG samples, the EEG channel is reinitialized and a new set of acquisitions are started. On the contrary, if a buffer overflow situation is expected, then, the stored data is transmitted towards the base-station. Meanwhile, the data previously received was already transferred from the base-station to the personal computer. This and the *modulation* scheme explain the nice shapes of the EEG signals depicted in Fig. 10. Fig. 10 shows for illustrations purpose, two EEG signals obtained with these IrO dry electrodes using a sampling frequency of 100 Hz, a selected passband in the range 1–30 Hz and a wireless transmission towards the base-station. Following the reception of radio-frequency signals and respective down-conversion to the base-band, the recovered EEG signals were sent trough the serial port to a personal computer for storing and displaying. The two EEG signals in Fig. 10 were obtained in two situations with the patient sitting in a chair, e.g., with the eyes opened and with the eyes closed, respectively. Fig. 10 also shows the amplitude spectrums of respective EEG signals, where one can observe two well defined peaks for the eyes-open situation.

The power consumptions in the WiDE-EEG are divided as follows: the acquisition system contributes with 10 mW per channel, whereas the MICAz module contributes with 57 mW (e.g., 24 mW from the microcontroller and 33 mW from the RF chip). The autonomy of the WiDE-EEG is about 25 h, when it is supplied by 2× AA 1.5 V battery.

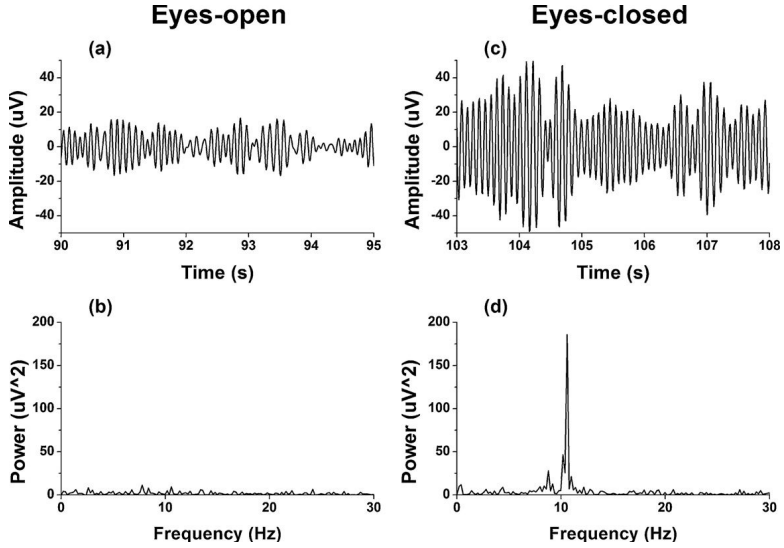

Fig. 10. The acquired EEG signal and respective amplitude spectrum with a sampling frequency of 100 Hz, a pass-band in the range 1–30 Hz, and with the individual with the eyes opened (plots on left) and closed (plots on right).

6. Comparison with the best state-of-the-art

Table 1 compares the WiDE-EEG with other solutions found on the very best state-of-the-art. Two types of solutions were analyzed, e.g., customized and COTS (commercial of-the-shelf) solutions. Table 1 shows that the WiDE-EEG is the solution for acquiring EEG signals that present the best global compromise between all the characteristics, e.g., the highest signal resolution, the highest signal gain, the best detectable signal, the highest baud-rate, and the most power-supply friendly apparatus. Also, the WiDE-EEG presents other acceptable characteristics as a whole for the target application, e.g., a reasonably acceptable number of analog channels, a small system clock frequency, moderate dimensions, and a good transmission range. Moreover, the most attractive characteristics of the WiDE-EEG are to be a solution for non-invasive EEG with neither skin abrasion nor electrolytic gel.

7. Conclusions

This paper presented a non-invasive wireless acquisition system (WiDE-EEG) for acquiring EEG signals with no need for electrode preparation. The WiDE-EEG can acquire EEG signals from up to 5 channels at a sampling rate of 1000 samples/s/channel to send them to a processing unit through RF in a 10 m range. The analog channels were optimized for acquiring EEG signals (with amplitudes up to 100 μV). Each analog channel can present the high signal gain of 66 dB, a common mode rejection ratio of 56.5 dB and a system resolution of 9.98 μV_{pp}. EEG electrodes with a three-dimensional structure (microtip) capable of bypassing the skin non-conductive layer, with a low resistance IrO film on its surface permits to the construction of a biopotential recording (and also for stimulating purposes) electrode with fast application. In conclusion, the use of dry IrO electrodes with the WiDE-EEG for acquiring EEG signals allow the patients to maintain their mobility while simultaneously having their electrical brain activity monitored.

Future designs will include the instrumentation amplifier model AD8236 for replacing the AD627 (also fabricated by the same manufacturer) for matching with the IEC60601 standard (the typical CMRR = 100 dB and minimum CMRR = 90 dB provided by the AD8236 for the same gain – i.e., 10 – ensures a CMRR higher or equal than the 90 dB imposed by the standard). The AD8236 instrumentation amplifier will also provide new attractive features such as: a low power consumption with the small absorbed current of 40 μA, low input currents (a maximum of 1 pA and 0.5 pA for the input bias current and for the input offset current, respectively). Also, a relaxation in the input amplifiers (with level shifting) will be expected because the new design will allow simultaneously rail-to-rail inputs and outputs and voltage operation in the range from 1.8 V to 5.5 V.

Conflict of interest statement

The authors declare that there are no conflicts of interest.

References

[1] Yoo S, Chong P, Kim D, Doh Y, Pham M, hoi E, et al. Guaranteeing Real-Time Services for Industrial Wireless Sensor Networks with IEEE 802.15.4. IEEE Transactions on Industrial Electronics 2010:1–11.

[2] Lee J, Kwon T, Song J. Group connectivity model for industrial wireless sensor networks. IEEE Transactions on Industrial Electronics 2010:1–21.

[3] Agha KA, Bertin M-H, Dang T, Guitton A, Minet P, Val T, et al. Which wireless technology for industrial wireless sensor networks? The development of OCARI technology. IEEE Transactions on Industrial Electronics 2009;56(October (10)):4266–78.

[4] Gungor VC, Hancke GP. Industrial wireless sensor networks: challenges, design principles, and technical approaches. IEEE Transactions on Industrial Electronics 2010;56(October (10)):4258–65.

[5] Guo H, Low K-S, Nguyen H-A. Optimizing the localization of a wireless sensor network in real time based on a low cost microcontroller. IEEE Transactions on Industrial Electronics 2010:1–9.

[6] Lu B, Gungor VC. Online and remote motor energy monitoring and fault diagnostics using wireless sensor networks. IEEE Transactions on Industrial Electronics 2009;56(October (10)):4651–9.

[7] Brandl M, Grabner J, Kellner K, Seifert F, Nicolics J, Grabner S, et al. A low-cost wireless sensor system and its application in dental retainers. IEEE Sensors Journal 2009;9(March (3)):255–62.

[8] Andre N, Druart S, Gerard P, Pampin R, Moreno-Hagelsieb L, Kezai T, et al. Miniaturized wireless sensing system for real-time breath activity recording. IEEE Sensors Journal 2010;10(January (1)):178–84.

[9] Liao HY, Chou J-C. Potentiometric multisensor based on ruthenium dioxide thin film with a bluetooth wireless and web-based remote measurement system. IEEE Sensors Journal 2009;9(December (12)):1887–94.

[10] Duun SB, Haahr RG, Birkelund K, Thomsen EV. A ring-shaped photodiode designed for use in a reflectance pulse oximetry sensor in wireless health monitoring applications. IEEE Sensors Journal 2010;10(February (2)):261–8.

[11] Exame Infomática July 2005:100–1 [in Portuguese].

[12] Lebedev A, Nicolelis MAL. Brain–machine interfaces: past, present and future. Trends in Neurosciences 2006;29(July (9)):536–46.

[13] Tallgren P, Vanhatalo S, Kaila K, Voipio J. Evaluation of commercially available electrodes and gels for recording of slow EEG potentials. Clinical Neurophysiology 2005;116(April (4)):799–806.

[14] Mahajan Y, McArthur G. Does combing the scalp reduce scalp electrode impedances? Journal of Neuroscience Methods 2010:1–3.

[15] Grimnes S, Martinsen ØG. Bioimpedance and bioelectricity basics. London, UK: Academic Press; 2000.

[16] Ollikainen JO, Vauhkonen M, Karjalainen PA, Kaipio JP. Effects of electrode properties on EEG measurements and a related inverse problem. Medical Engineering & Physics 2000;22(October (8)):535–45.

[17] Beck N, Johnson I. Shaping TinyOS to deal with evolving device architectures: experiences porting TinyOS-2.0 to the Chipcon CC2430. In: Proc. of the 4th workshop on embedded networked sensors. 2007. p. 83–7.

[18] Patnode D, Dunne J, Malinowski A, Schertz D. WISENET – TinyOS based wireless network of sensors. In: Proc. of the 29th annual conference of the IEEE industrial electronics society, IECON'03, vol. 3. 2003. p. 2363–8.

[19] Crossbow, Inc., http://www.xbow.com/.

[20] van Hoesel L, Havinga P. A lightweight medium access protocol (LMAC) for wireless sensor networks. In: Proc. of first international workshop on networked sensing systems (INSS 2004). 2004.

[21] Carmo JP, Dias NS, Silva HR, Mendes PM, Couto C, Correia JH. A 2.4-GHz low-power/low-voltage wireless plug-and-play module for EEG applications. IEEE Sensors Journal 2007;7(November (11)):1524–31.

[22] Dias NS, Carmo JP, Mendes PM, Correia JH. A low power/low voltage CMOS wireless interface at 5.7 GHz with dry electrodes for cognitive networks. IEEE Sensors Journal 2011;11(March (3)):755–62.

[23] Zhu W, White MJ, Nellis GF, Klein SA, Gianchandani YB. A Si/glass bulk-micromachined cryogenic heat exchanger for high heat loads: fabrication, test, and application results. IEEE Journal of Microelectromechanical Systems 2010;19(January (1)):38–47.

[24] Dean RN, Luque A. Applications of microelectromechanical systems in industrial processes and services. IEEE Transactions on Industrial Electronics 2009;56(April (4)):913–25.

[25] Seidel H, Csepregi L, Heuberger A, Boumgärtel H. Anisotropic etching of crystalline silicon in alkaline solutions: orientation dependence and behavior of passivation layers. Journal of Electrochemical Society 1990;137(November (11)):3612–26.

[26] Chen T, Chen L, Sun L, Li X. Design and fabrication of a four-arm-structure MEMS gripper. IEEE Transactions on Industrial Electronics 2009;56(April (4)):996–1004.

[27] Frazier AB, Warrington RO, Friedrich C. The miniaturization technologies: past, present, and future. IEEE Transactions on Industrial Electronics 1995;42(May (5)):423–30.

[28] van der Pauw LJ. A method of measuring the resistivity and Hall coefficient on lamellae of arbitrary shape. Philips Technical Review 1958;20:220–4.

[29] Dias NS, Carmo JP, Ferreira da Silva A, Mendes PM, Correia JH. New dry electrodes based on iridium oxide (IrO) for non-invasive biopotential recordings and stimulation. Journal Sensors and Actuators A 2010;164:28–34.

[30] Afonso JA, Macedo P, Silva HD, Correia JH, Rocha LA. Design and implementation of multi-user wireless body sensor nNetworks. Journal on Advances in Networks and Services, IARIA Publisher 2010:62–74.

[31] Pattan B. Robust modulation methods and smart antennas in wireless communications. Prentice Hall; 1999.

[32] Hummels DR, Ratcliffe FW. Calculation of error probability for MSK and OQPSK systems operating in a fading multipath environment. IEEE Transactions on Vehicular Technology 1981;3(August (30)):112–20.

[33] Modarreszadeh M, Schmidt RN. Wireless 32-channel, EEG and epilepsy monitoring system. In: Proc. 19th international conference of the IEEE engineering in medicine and biology society. 1997. p. 1157–60.

[34] Chi YM, Cauwenberghs G. Wireless non-contact EEG/ECG electrodes for body sensor networks. In: Proc. 2010 international conference on body sensor networks (BSN). 2010. p. 297–301.

[35] Farshchi S, Mody I, Judy JW. A TinyOS-based wireless neural interface. In: Proc. 26th international conference of the IEEE engineering in medicine and biology society. 2004. p. 4334–7.

[36] Obeid I, Nicolelis MAL, Wolf PD. A multichannel telemetry system for single unit neural recordings. Journal of Neural Methods 2004;133:33–8.

[37] Ye X, Wang P, Liu J, Zhang S, Jiang J, Wang Q, et al. A portable telemetry system for brain stimulation and neuronal activity recording in freely behaving small animals. Journal of Neuroscience Methods 2008;174:186–93.

[38] Takeuchi S, Shimoyama I. A radio-telemetry system with a shape memory alloy microelectrode for neural recording of freely moving insects. IEEE Transactions on Biomedical Engineering 2004;51(January (1)):133–7.

[39] Irazoqui-Pastor P, Mody I, Judy JW. Transcutaneous RF-powered neural recording device. In: Proc. 24th annual conference/annual fall meeting IEEE biomedical engineering society. 2002. p. 23–6.

Nuno Sérgio Dias (S'06) graduated in Industrial Electronics and Computers at University of Minho, Portugal in 2004. In 2009, he obtained the PhD degree in Industrial Electronics from the University of Minho, Guimarães, Portugal, in collaboration with the Center for Neural Engineering at The Pennsylvania State University, State College, PA, USA. His PhD thesis was on Brain–Machine Interface Based on Biotelemetry and Dry Electrodes. He is currently pursuing a Post-Doc Researcher at Life and Health Sciences Research Institute – ICVS, University of Minho, Braga, Portugal. Doctor Dias is also a Member of the IEEE Industrial Electronics Society, and of the IEEE Engineering in Medicine and Biology Society.

João Paulo Carmo (S'02–M'08) was born in 1970 at Maia, Portugal. He graduated in 1993 and received his MSc degree in 2002, both in Electrical Engineering from the University of Porto, Porto, Portugal. In 2007, he obtained the PhD degree in Industrial Electronics from the University of Minho, Guimarães, Portugal. His PhD thesis was on RF transceivers for integration in microsystems to be used in wireless sensors network applications. Since 2008, he is a principal researcher at the Algoritmi Center, University of Minho, Guimarães, Portugal. He is involved in the research on micro/nanofabrication technologies for mixed-mode/RF systems, solid-state integrated sensors, microactuators and micro/nanodevices for use in wireless and biomedical applications. Doctor Carmo is also involved with the supervision of PhD students from the MIT-Portugal program. He is member of the IEEE Industrial Electronic Society and performs regular reviews on these publications: IEEE Sensors Journal, IEEE Transactions on Industrial Electronics, IEEE Transactions on Industrial Applications, IEEE Transactions on Transactions on Neural Systems and Rehabilitation Engineering, Elsevier Microelectronics Journal, Elsevier Journal of Sensors and Actuators (Physical sensors), Journal of Measurement Science and Technology (Institute of Physics), Journal of Physiological Measurement (Institute of Physics), The IET (Electronic Letters and Journal of Wireless Sensors Systems). He is also a regular collaborator integrating the technical committees of the international conferences Eurosensors (anual European Conference on Sensors), Microelectromechanical Europe (MME), confTele (Conference on Telecommunications, a Portuguese biannual conference), IEEE Industrial Electronics Society Annual Conference (IECON), IEEE International Symposium on Industrial Electronics (ISIE), as well as of the Symposium on Microelectronics Technologies and Devices (SBMicro, a Brazilian annual conference). Finally, he is co-author of the book entitled *Introdução às microtecnologias no Silício*, published by LIDEL Editors (Lisbon, Portugal).

Paulo Mateus Mendes (M'05) graduated in 1995, and obtained his MSc degree in Electrical Engineering, in 1999, both from University of Coimbra, Portugal. He obtained his PhD degree in Industrial Electronics, from University of Minho, in 2005. Since 2006 he has been an Assistant Professor at University of Minho, and a researcher at the Algoritmi Center. He has been involved in several projects related to project, fabrication, and characterization of microantennas for wireless microsystems. Doctor Mendes is Member of the European Microwave Association, of the IEEE Antennas and Propagation Society, and of the IEEE Engineering in Medicine and Biology Society.

José Higino Correia (S'96–M'00) graduated in Physical Engineering from University of Coimbra, Portugal in 1990. He obtained in 1999 a PhD degree at the Laboratory for Electronic Instrumentation, Delft University of Technology, The Netherlands, working in the field of microsystems for optical spectral analysis. Presently, he is a Full Professor in Department of Industrial Electronics, University of Minho, Portugal. He was the General-Chairman of Eurosensors 2003 and MME 2007, Guimarães, Portugal. His professional interests are in micromachining and microfabrication technology for mixed-mode systems, solid-state integrated sensors, microactuators and microsystems. Professor Correia is also a Member of the IEEE Industrial Electronics Society.